



Ab initio simulation of amorphous GeSe₃ and GeSe₄

R. Thapa^{a,*}, C. Ugwumadu^a, K. Nepal^a, D.A. Drabold^b, M.T.M. Shatnawi^c

^a Department of Physics and Astronomy, Nanoscale and Quantum Phenomena Institute (NQPI), Ohio University, Athens, OH 45701, USA

^b Department of Physics and Astronomy, Ohio University, Athens, OH 45701, USA

^c Physics Department, The University of Jordan, Amman 11942, Jordan

ARTICLE INFO

Keywords:

Chalcogenide glasses

FEAR

Ab initio methods

ABSTRACT

The structural, vibrational, and electronic properties of glassy GeSe₄ were studied, in conjunction with GeSe₃, using an approach combining Reverse Monte Carlo with density functional theory total energies and forces. The models generated using the force enhanced atomic refinement (FEAR) technique showed close agreement with both X-ray and neutron diffraction data while sitting in a deep enough energy minimum defined by accurate interatomic interactions. These models produced important structural features of the system like the Ge–Ge correlations and the first sharp diffraction peak (FSDP) and is in better agreement to the experiment compared to the melt-quench (MQ) model.

1. Introduction

Modeling of atomic-scale structure and ordering in amorphous materials has been an area of active research for many decades now [1]. It follows that an understanding of the basic architecture of a material creates an avenue for optimization of the material for wider applications. One material that has enjoyed tremendous scientific interest is the glassy Germanium Selenide materials, g-Ge_xSe_{1-x} (0 ≤ x ≤ 1). These materials can be made in glassy state over a wide range of x (0 < x < 0.43) [2], and reveal scientifically important ordering on the atomic scale [3–6]. This has also gathered a lot of attention because the connectivity of the covalently bonded network can be changed by altering the Ge:Se ratio over the glass forming region. Chalcogenide glasses are known to exhibit a wide range of physical properties like high linear and non-linear refractive indices, large infrared transparency, and reversible amorphous to crystalline transition [7]. GeSe₄ (x = 0.2) and GeSe₃ (x = 0.25) are important starting material in many opto-electronic applications, for example, purifying Se before glass synthesis of g-GeSe₄ fibers, used in optical telecommunication, notably reduces optical losses in the mid-IR range [8]. This property also extends to GeSe₃ which has low optical absorption due to its wide band-gap and configurable optical properties [9]. Using noble metals (notably Ag) as an additive to GeSe glasses forms a useful material for conducting bridge memory (CBRAM) devices, an ultra-low power non-volatile memory technology [10–12]. GeSe glasses form an ideal system to study the floppy to rigid transition with an increase in the mean coordination as proposed by the constraint counting theory [13,14].

As pointed out by Thorpe [15], the rigidity percolation occurs at a mean coordination of 2.4, corresponding to GeSe₄, where the network transforms from floppy to rigid with the transition being accompanied by abrupt changes in several physical properties [16–18].

For amorphous materials in general, accurate description of its vibrational, electronic and optical properties is heavily dependent on the availability of high quality structural models. For example, models generated solely from molecular dynamics (MD) not only suffer from short simulation times, but also produce unrealistic coordination defect concentration [19]. However, several sophisticated models for GeSe glasses exist which give better account of the structural properties of the material [20–23], but the hybrid functionals used for those models are computationally expensive and most fail at reproducing the experimental Ge–Ge correlation function which is specified by the so-called first sharp diffraction peak (FSDP). For chalcogenide glasses with small Ge concentration, the Ge–Ge correlation function gives information on the Ge — centered structural motifs and hence contributes substantially to features of the model (i.e. from the exchange and correlation energy functional used [22,24,25] to the system size and residual pressure effects [26]). It is noteworthy that efforts are being made to improve the Ge–Ge correlation function, for example; Chaker and co-workers [27] incorporated Van der Waals dispersion forces into first-principle molecular dynamics simulations (FPMD) with BLYP (Becke, Lee, Yang and Parr) exchange–correlation functional [28,29]; while this requires additional calculations, it showed that Ge–Ge correlation is sensitive to the kind of dispersion force considered. Therefore, since

* Corresponding author.

E-mail addresses: rt887917@ohio.edu (R. Thapa), cu884120@ohio.edu (C. Ugwumadu), kn478619@ohio.edu (K. Nepal), drabold@ohio.edu (D.A. Drabold), moneeb.shatnawi@ju.edu.jo (M.T.M. Shatnawi).

<https://doi.org/10.1016/j.jnoncrysol.2022.121998>

Received 8 April 2022; Received in revised form 21 September 2022; Accepted 25 October 2022

Available online 26 November 2022

0022-3093/© 2022 Elsevier B.V. All rights reserved.

different conclusions can be inferred from the available models with regard to the network structure of g-GeSe₄ as well as g-GeSe₃ due to the inaccuracy in reproducing the Ge–Ge correlation function or some other features, a break-through would be providing a model that can be consistent with all measured partial pair correlation function as well as experimental data.

The composition GeSe₄ is of special interest in the study of the floppy to rigid transition because this composition is the boundary between the two states, corresponding to mean coordination number 2.4 calculated with the 8-N rule [30]. Therefore, one might expect vibrational signatures to change significantly near this composition especially for the low frequency ($\omega \rightarrow 0$) limit. While the constraint counting theory is foundational contribution to our understanding of these materials, it is also idealized: it is based on a mean field theory and ignores forces other than stretching and bending forces from idealized bonds. In our work, we do not make these approximations, so that similarities and differences between the idealized and more realistic systems are of interest.

Several attempts to theoretically model the structure of GeSe₄ has been made in the past ranging from RMC simulations [5,31–34] to classical molecular dynamics [35–37] to complex density functional theory based calculation with different exchange and correlation functional [20,22,27,38]. An approach to simulating an acceptable model which can be used to explore structure-based properties of g-GeSe₄, as well as address the discrepancies between experiment and prediction of the Ge–Ge correlation function without using computationally expensive hybrid functional involves: (i) directly using available experimental information through the Reverse Monte Carlo (RMC) technique [39]. (ii) a systematic minimization of the total energy of the configuration as well as the discrepancies in the atomic coordinates (caught by RMC) focused at increasing the probability of the system settling on a global minimum. This method of teaching some chemistry to the RMC is termed force enhanced atomic refinement (FEAR) [40–42]. In this work, we use X-ray diffraction (XRD) data [43] to construct realistic models for (g-GeSe₄) and (g-GeSe₃) and compare the results obtained with previous theoretical calculations and experiments whenever possible. The models produced, in decent sizes, will be used to study the network topology in both the short and intermediate range.

2. Methodology and models

We prepare models of GeSe₃ (384 atoms at 4.31 g/cm³ [26]) and GeSe₄ (400 atoms at 4.38 g/cm³ [44]) at experimental densities using FEAR [40–42]. FEAR is a well-developed method for generating computer models for a wide variety of materials ranging from α -Si and α -SiO₂ to sodium silicates [45] and complex bulk metallic glass [46]. Well-equilibrated liquid melts, at 2000 K for 10 ps, of the models generated using the *building block* [19,47] method were used as starting configuration for the FEAR method discussed elsewhere [40]. FEAR is a successful technique to jointly satisfy structure factor data while at the same time producing a configuration that is a suitable energy minimum according to VASP. The experimental structure factor used was measured using high energy X-ray diffraction carried out at the Advanced Photon Source (APS), Argonne National Laboratory [43]. The energy minimization step used conjugate gradient (CG) algorithm in the projector augmented wave [48] implementation of the *ab initio* plane wave density functional theory package VASP [49–51] with Perdew–Burke–Ernzerhof [52] method as the exchange–correlation functional.

To compare/validate our findings from the FEAR models, we created a melt-quench (MQ) [19] models of the glasses with the same density using VASP. This model started with a random configuration of atoms, with no atoms closer than 2.0 Å from other atoms, and was heated to 2000 K in 9 ps where it was equilibrated for 15 ps. The equilibrated melt was cooled to 1000 K in 20 ps followed by a 10 ps equilibration at 1000 K. It was then cooled down to 300 K in 28

ps and was equilibrated at 300 K for 7 ps. The final models were then relaxed with CG algorithm to minimize the forces on each atom. Parallel FEAR calculations on smaller models (240 atom GeSe₄ and 300 atom GeSe₃) produced energy optimized structures but the agreement with the experimental X-ray structure factor and the radial distribution function was not on the same level as with the larger models.

3. Results and discussion

3.1. Structural properties

The total X-ray structure factor obtained from the models is shown in Fig. 1, along with the experiment data [43] for comparison. FEAR models show modest agreement with the experimental results [43] and the most significant difference between the FEAR and the MQ models is the presence of a pre-peak at 1.15 Å⁻¹, although not matching the experimental intensity, in the FEAR model. This peak is the first sharp diffraction peak (FSDP) and is related to ordering of atoms in the intermediate range [26,53]. Since, this FSDP arises mainly from the Ge–Ge correlations [26], a FSDP mismatch of the model with the experiment results in wrong Ge–Ge correlations as seen in the RDF of the MQ model. The comparison of total neutron structure factor obtained from the model with the experimental data [26], shown in Fig. 2, also shows that the FEAR models align closer to the experiment compared to the MQ models, markedly in the region around the FSDP.

The arrangement of atoms in real space and thus the bonding environment is studied using the radial distribution function (RDF) defined as:

$$g(r) = \frac{N}{4\pi r^2 V} \frac{dn(r)}{dr} \quad (1)$$

where N and V denote the total number of atoms and the volume of the simulation box respectively. $dn(r)$ denotes the number of atoms located at distances lying between r and $r+dr$. The radial distribution function (gr) gives the probability of finding an atom in a shell of thickness dr at a distance r from a reference atom. Since our models had two species, we also calculated the partial radial distribution function defined as:

$$g_{\alpha\beta}(r) = \frac{N c_{\alpha}}{4\pi r^2 V} \frac{dn_{\alpha\beta}(r)}{dr} \quad (2)$$

where c_{α} is the concentration of α atomic species. The functions $g_{\alpha\beta}(r)$ enable the computation of the probability of finding an atom of type β at a distance r from the reference α atom. To calculate the total and partial RDF both FEAR and MQ models were taken through an NVT ensemble at 300 K and the results were averaged over 2500 configurations collected over the final 5 ps of the simulation. The partial and total RDF from our models, plotted in Fig. 3, are in close agreement with the experimental results obtained using neutron diffraction with isotope substitution [26]. The absence of Ge–Ge homopolar bonds (correlations below 3 Å) in GeSe₄ observed in the neutron diffraction experiment [26] is exactly reproduced in our GeSe₄ model. The position of the peaks in the partial RDF and the mean coordination number, outlined in Table 1 agree with available experiments.

In general, the models produce reasonable agreement with the experiment in terms of the Ge–Se and Se–Se correlations. However, the Ge–Ge correlations, which is highly sensitive to the choice of the modeling procedure, differ between the MQ and FEAR models. The dependence of the Ge–Ge correlations on the exchange and correlation energy functional used in the simulations [24,25], the system size, and the quench protocol used [23,54] have been previously reported. This absence of Ge–Ge correlations in GeSe₄, also observed experimentally [26], indicates the absence of Ge–Ge homopolar bonds, i.e. Ge atoms bond only to Se atoms. The first peak in the total RDF of GeSe₄ arises from first neighbor correlations between the atoms within a structural motif. Thus, Fig. 3 suggests that there is no Ge–Ge correlations in GeSe₄ model for the FEAR model but such a correlation exists, even though small, for the MQ model. This finding also accounts for

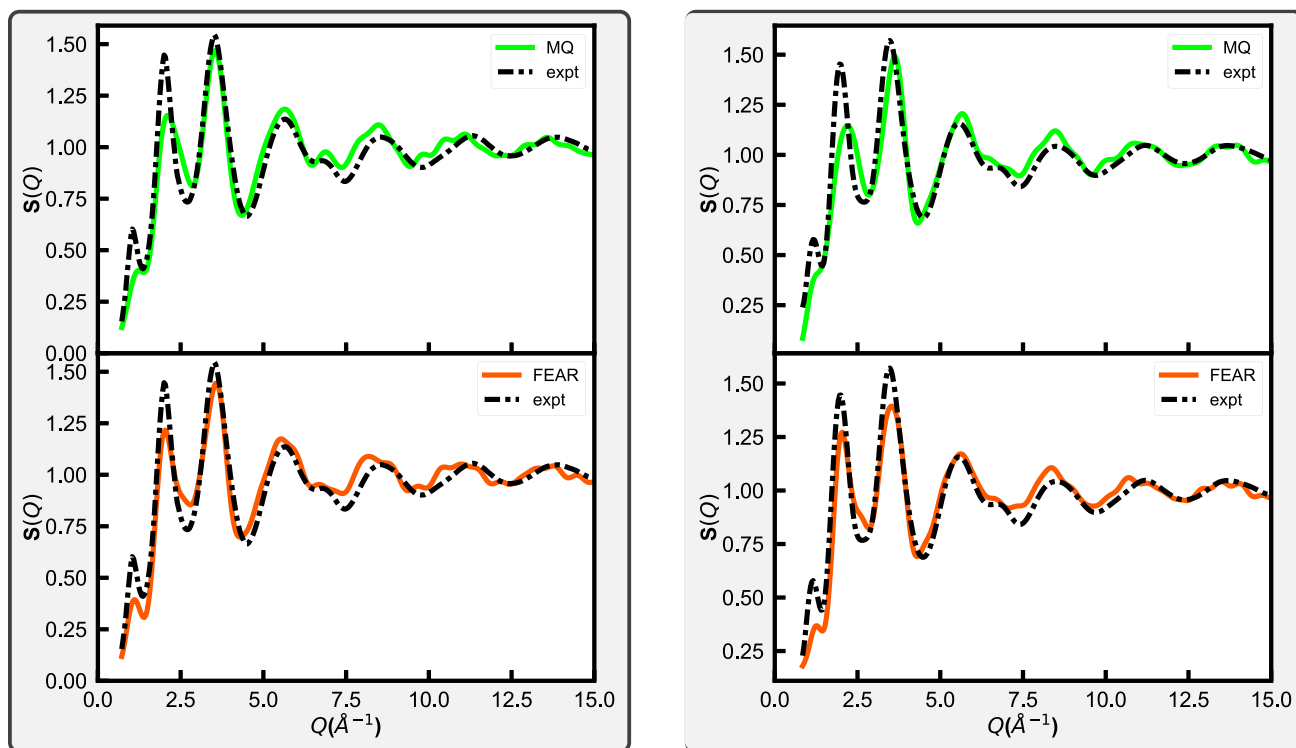


Fig. 1. Total X-ray structure factor of the MQ and FEAR models of GeSe_3 (left panel) and GeSe_4 (right panel) compared with experimental results from Moneeb et al. [43].

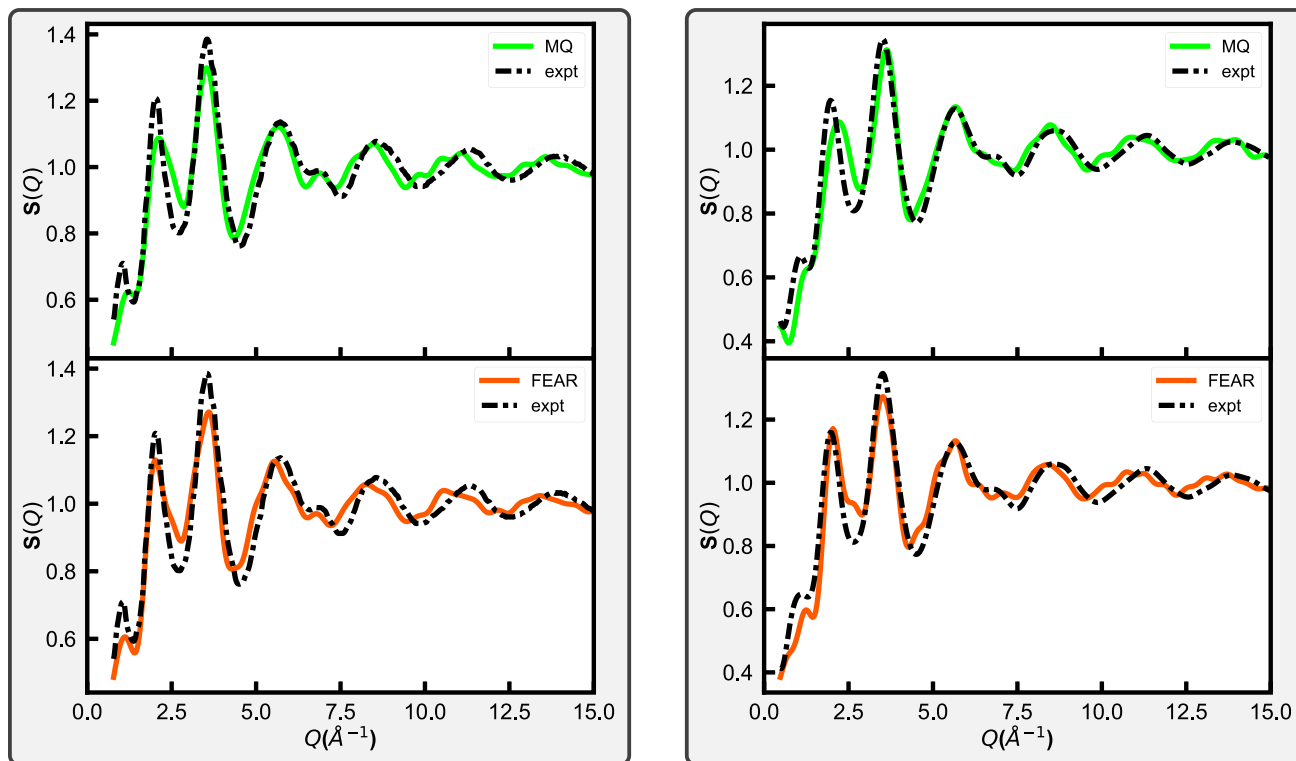


Fig. 2. Total neutron structure factor of the MQ and FEAR models of GeSe_3 (left panel) and GeSe_4 (right panel) compared with experimental results from Rowlands et al. [26].

the discrepancy in the intensity of the first peak between the MQ and FEAR models of GeSe_4 . Experimental evidences have shown that there is no Ge-Ge correlations in GeSe_4 [26].

The structure of GeSe_3 and GeSe_4 can be viewed as a collection of Ge centered tetrahedra connected to each other by Se atoms in

various fashion namely edge shared (ES) and corner shared (CS). The frequency of occurrence of Se-Se homopolar bonds and the length of Se chains positively correlates with the Se concentration. Our models for GeSe_3 and GeSe_4 show four distinct Se environments: Ge-Se-Se, Se-Se-Se, and Ge-Se-Ge where the Se atom is shared by two Ge(Se)₄

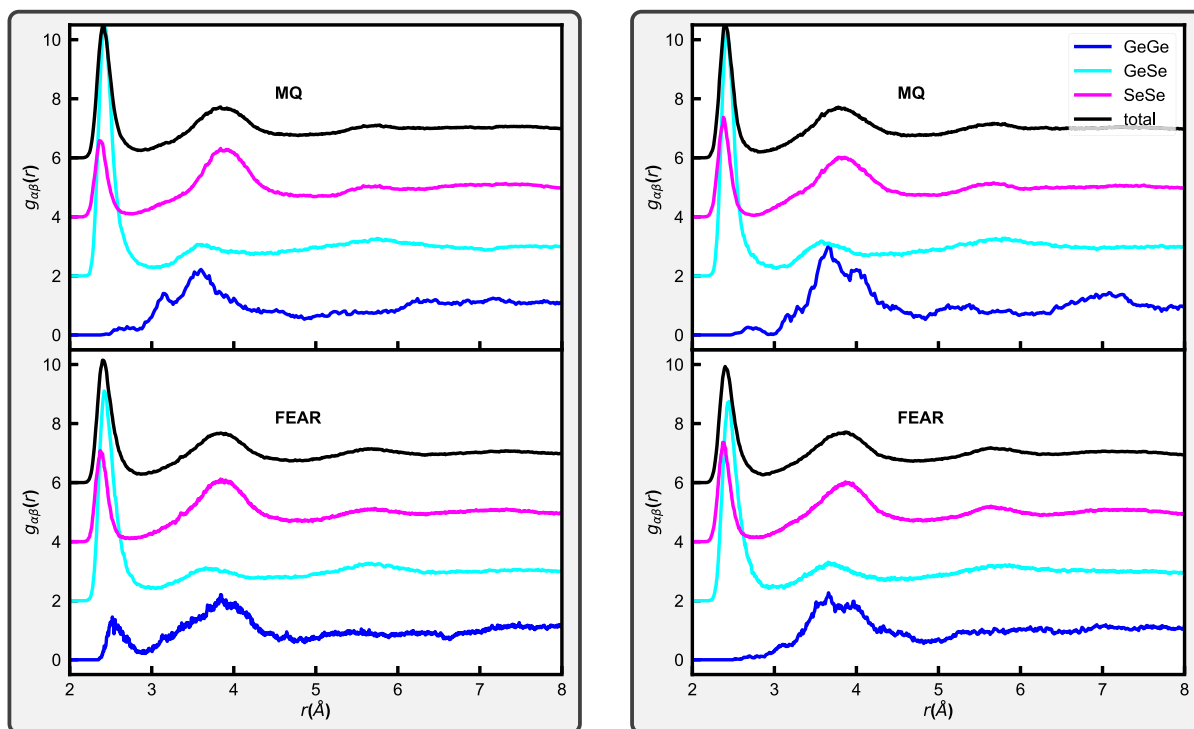


Fig. 3. Partial radial distribution function of the MQ and FEAR models of GeSe₃ (left panel) and GeSe₄ (right panel). The RDF's have been shifted vertically for clarity.

tetrahedra connected either in CS or ES fashion. This finding is in line with NMR experiments on these materials [55]. The comparison of real and reciprocal space information for GeSe₃ and GeSe₄ shows that an increase in Ge-Se content within the intermediate phase (IP) creates an additional length scale in the atomic ordering associated with the intermediate range order arising from the connection of Ge atoms in neighboring tetrahedra [56]. This manifests as a peak in the Ge-Ge correlation in the GeSe₃ and as a FSDP, with higher intensity compared to GeSe₄, in the S(Q). To study the difference in the Ge-Ge connectivity between GeSe₃ and GeSe₄, we calculated the statistics of the different modes of connections between the Ge-centered motifs: namely corner-shared and edge-shared, and tabulated in Table 2. The table shows a significant increase in the connectivity between Ge-atoms, both CS and ES, as we go from GeSe₄ to GeSe₃. This can be thought of as the added Ge atoms trying to break up and crosslink the Se chain structures by forming four-fold coordinated Ge-centered structural motifs [56]. Also, the ratio of ES:CS tetrahedra in GeSe₃ is in close agreement with results from MAS NMR experiment [55]. The frequency of the length of most frequent isolated Se chains, made with Se atoms that are not bonded to Ge, listed in Table 2 suggests that the addition of Ge atoms to GeSe₄ breaks the Se chain links to form cross-linking connections and a more rigid network topology. The number of Ge-Ge bonds reported in Table 2 for GeSe₄ agrees well with the Ge-Ge coordination number reported in Rowlands et al. [26].

The atomic correlation further than the nearest neighbor was analyzed on the CG relaxed model using the ring statistics algorithm that has been applied to both compositions using the ISAACS code. The bond cutoff distances between atomic pairs are determined by the first minima of the partial RDF and are different for GeSe₃ and GeSe₄. Within ISAACS, we used the algorithm developed by King [57] and later updated by Franzblau [58]. As seen in Fig. 4, there is a significant difference in the distribution of the rings between the two compositions. These results are in significant agreement with previous DFT calculations [20]. The increase in the number of 4-fold rings in GeSe₃ is attributed to the higher fraction of ES Ge(Se)₄ tetrahedral connections compared to GeSe₄.

Table 1

Position of the first peak ($R_{\alpha\beta}$) (in Å) in partial correlations calculated from FEAR models of GeSe₃ and GeSe₄. The quantities in the brackets are taken from neutron diffraction study by Rowlands et al. [26]. The average coordination number (\bar{n}) for each model is also listed.

	GeSe ₃	GeSe ₄
R_{GeGe}	2.55	
R_{GeSe}	2.42 (2.37)	2.44 (2.37)
R_{SeSe}	2.40 (2.34)	2.37 (2.35)
\bar{n}	2.50	2.38
$\bar{n}(8-N)$	2.50	2.40

Table 2

Statistics of the Ge-Ge connectivity in GeSe₃ and GeSe₄ calculated using Ge-Se bond length of 2.90 Å. Ge atoms are considered bonded if they are less than 2.90 Å apart. The number of ES, CS connections are normalized by the number of Ge-atoms in the models. The number of the most frequent isolated Se-chains with different lengths n_{Se_n} is also listed.

	GeSe ₃	GeSe ₄
CS	1.030	0.750
ES	0.135	0.125
n_{GeGe}	14	0
n_{Se_4}	9	13
n_{Se_5}	6	8
n_{Se_6}	1	3

The bond angle distribution (BAD) is also studied to understand the local structure around the Ge(Se)₄ tetrahedra and the way they are connected. The Se-Ge-Se BAD is peaked at around 110° indicating the presence of tetrahedral order [20]. In Fig. 5, the Ge-Se-Ge BAD, arising from connection between the tetrahedra, has clear peaks at ~80° and ~100° assigned to ES and CS tetrahedra, respectively. The intensity of the ES peak appears to be inversely proportional to the Ge content as previously observed [20]. This dominance of ES units is larger in GeSe₃ which can also be seen from the ring statistics (see Fig. 4).

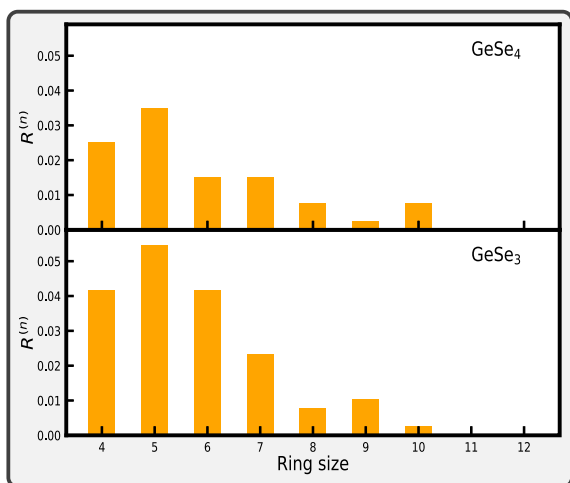


Fig. 4. Distribution of rings of different size in the models calculated using ISAACS [59]. Bond cutoff are taken from the first minimum of RDF.

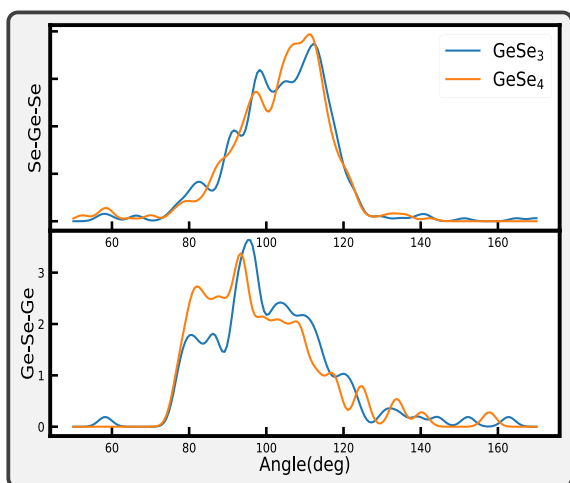


Fig. 5. Bond angle distributions in the models computed for Ge–Se–Ge and Se–Ge–Se. The BAD has been Gaussian broadened (with $\sigma = 2.5^\circ$).

3.2. Electronic properties

The electronic structure was studied using the total density of states (DoS), partial DoS, and inverse participation ratio (IPR). These quantities help us in several ways — validate/invalidate the models, understand the conducting/insulating behavior, and study the extent of localization of electronic states. The conduction in amorphous systems depends mainly on the density of states and the extent of localization of the Kohn–Sham states near the Fermi level. An account of the localization of Kohn–Sham states is given by IPR defined as:

$$I(\psi_n) = \frac{\sum_i |a_n^i|^4}{(\sum_i |a_n^i|^2)^2} \quad (3)$$

where a_n^i is the contribution to the eigenvector ψ_n from the i th atomic orbital (s, p, and d) as calculated with VASP. Putting the definition in simpler terms, localized states have high IPR value (ideally equal to $I = 1$) while a completely extended state having a value of $(1/N)$, i.e. evenly distributed over N atoms. From Fig. 6, we observe that our models have low DoS near the Fermi level. Furthermore those states are highly localized, as suggested by higher values of IPR. The combined effect of these findings suggests that the models are non-conducting. Furthermore, the partial DoS plots show that the significant contribution to the DoS comes from the Se atoms in both models. In

order to understand the origin of the localized states near the Fermi level, we show the atomic projection of four such states onto the atoms in Fig. 7. As expected for localized states, the states are highly localized on few atoms. Furthermore, these localized states arise mostly from the Se chain links in the network which is also seen in the partial DoS in Fig. 6.

3.3. Vibrational properties

The analysis of the vibrational properties of amorphous materials not only provides a useful insight to the local bonding environment but also helps understand the thermal and mechanical properties. Vibrational properties of the models were studied using the harmonic approximation. The Hessian matrix is computed by displacing each atom in 6-directions ($\pm x, \pm y, \pm z$) by 0.015 \AA . The few lowest frequencies arising from rigid supercell transitions were removed from the calculations of the vibrational density of states (VDoS). The VDoS is defined as:

$$g(\omega) = \frac{1}{3N} \sum_{i=1}^{3N} \delta(\omega - \omega_i) \quad (4)$$

with N and ω_i representing the number of atoms and the eigenfrequencies of normal modes, respectively. This definition suggests that any frequency that has larger number of eigenfrequencies in its neighborhood will have a higher VDoS. The delta function is approximated by a Gaussian with a standard deviation of 1.5% of the maximum normal mode frequency.

The extent of localization of each normal mode frequency is studied using the vibrational inverse participation ratio (VIPR) defined as:

$$\mathcal{V}(\omega_n) = \frac{\sum_{i=1}^N |\mathbf{u}_n^i|^4}{(\sum_{i=1}^N |\mathbf{u}_n^i|^2)^2} \quad (5)$$

where \mathbf{u}_n^i is displacement vector of i th atom at normal mode frequency ω_n . By definition, low values of VIPR indicate vibrational mode evenly distributed among the atoms while higher values imply only a few atoms contributing at that particular eigenfrequency.

The total and partial VDoS plotted in Fig. 8 agree reasonably well with previous calculations on the materials [20,61] showing a broad band centered at $\sim 80 \text{ cm}^{-1}$ for both models and matching subsequent peak positions. The low frequency peak at $\sim 50 \text{ cm}^{-1}$ arises mainly from the floppy modes arising from the vibrations among the loosely bound Se-atoms. As suggested by VIPR, these low frequency floppy modes are highly delocalized and shared by a large number of Se-atoms. Sub peaks at $\sim 160 \text{ cm}^{-1}$ and $\sim 250 \text{ cm}^{-1}$, arising from bond-bending and bond stretching vibrational modes respectively, have been previously reported [61]. The Se rich GeSe_4 has a higher intensity of the high frequency motion associated with the A_{1c} mode arising from the atomic motion of Se atoms connecting edge-shared tetrahedra [62]. This can be viewed as an effect of increased concentration of the ES tetrahedral connection in GeSe_4 compared to GeSe_3 , a finding also seen in the ring statistics analysis above. To facilitate a visual interpretation of the different kinds of vibrational modes present in the system, we have included animations of representative modes along with this manuscript.

4. Conclusion

We generated realistic GeSe glasses in the intermediate range using experimental X-ray diffraction measurements. The models produced showed good agreement with the experiment even without the use of hybrid functional calculations. The structural, electronic, and vibrational signature of the models were parallel with previous theoretical and experimental studies. The Ge–Ge correlations in these glasses matched significantly well with experiments. This is a clear advantage of the FEAR over the MQ technique because FEAR injects the experimental information into the model in each step. As we moved from GeSe_4 to GeSe_3 , we saw clear signature of breaking of Se chains and formation of cross-linking connections to form a more rigid topology.

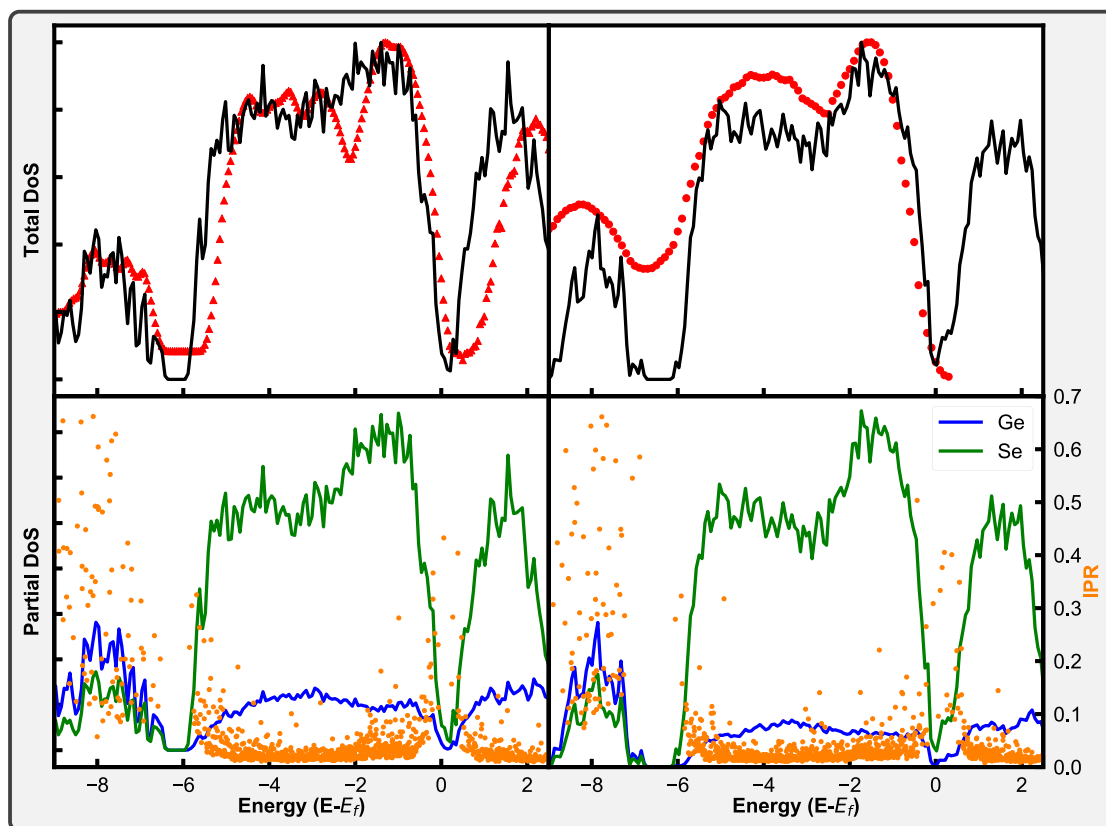


Fig. 6. Total and partial Electronic DoS and Inverse Participation Ratio (IPR) calculated for GeSe_3 (left) and GeSe_4 (right) models. The results are compared with photoemission spectroscopy (red circles) [60] and previous simulation result (red triangle) [20].

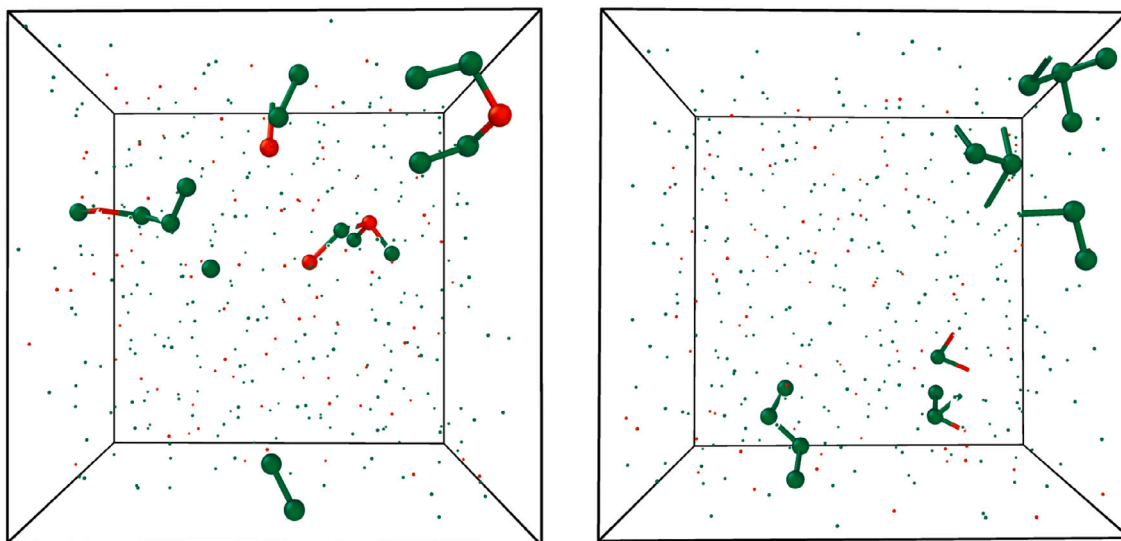


Fig. 7. Projection of the localized states near the Fermi level onto atoms in GeSe_3 (left) and GeSe_4 (right) models. Red and green atoms indicate Ge and Se atoms respectively. Only few atoms with higher projection of the states on them are shown.

Data availability

Data will be made available on request.

Acknowledgments

This work used the Extreme Science and Engineering Discovery Environment (XSEDE), which is supported by National Science Foundation, USA grant number ACI-1548562. We acknowledge the computational resources provided to us through XSEDE under the allocation

number DMR-190008P. I express my sincere gratitude to Donald Roth for setting up and maintaining the computational resources.

Appendix A. Supplementary data

Supplementary material related to this article can be found online at <https://doi.org/10.1016/j.jnoncrysol.2022.121998>.

Visual representation of different kinds of normal mode vibrations of atoms in the model. The low frequency modes come from the floppy vibrational modes.

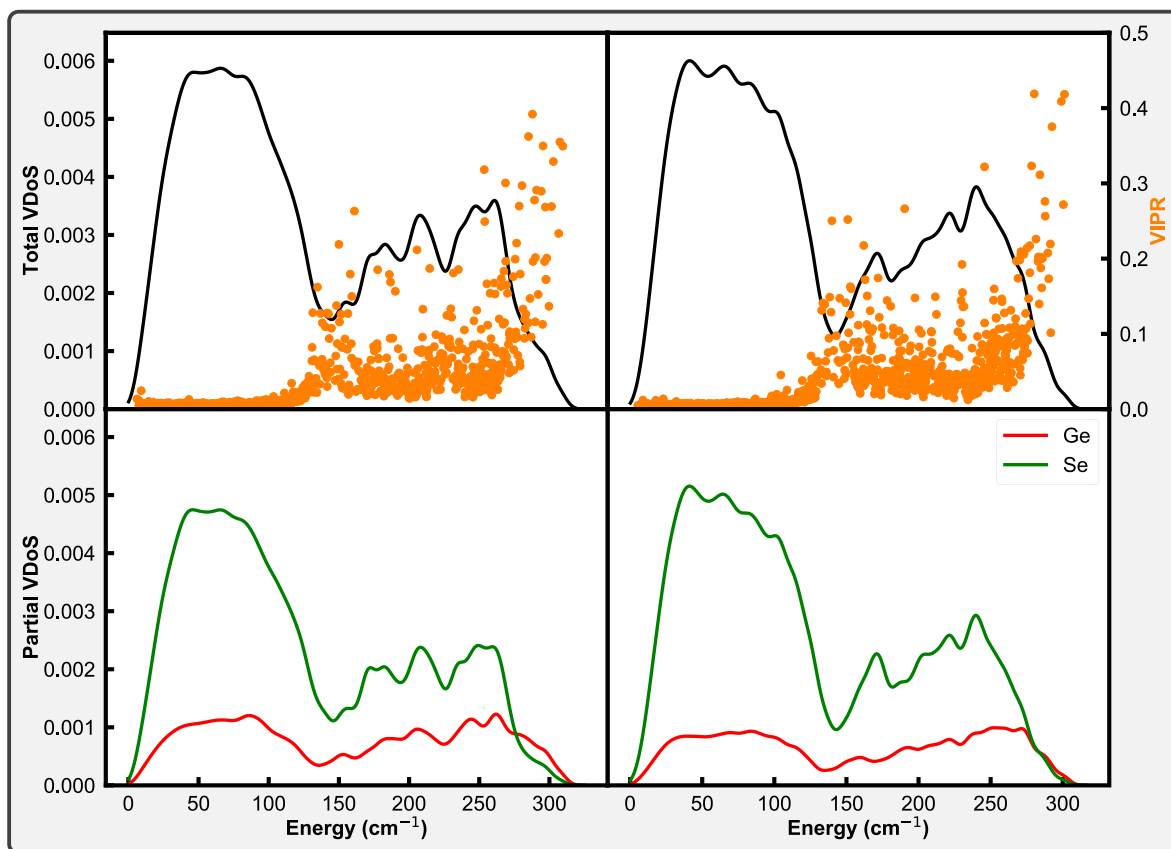


Fig. 8. Total and partial VDoS and VIPR calculated for GeSe_3 (left) and GeSe_4 (right) models.

References

- [1] L.J. Lewis, *J. Non-Cryst. Solids* 580 (2022) 121383.
- [2] R. Azoulay, H. Thibierge, A. Brenac, *J. Non-Cryst. Solids* 18 (1975) 33–53.
- [3] D.A. Whittaker, L. Giacomazzi, D. Adroja, S.M. Bennington, A. Pasquarello, P.S. Salmon, *Phys. Rev. B* 98 (2018) 064205.
- [4] A. Zeidler, P.S. Salmon, D.A. Whittaker, K.J. Pizzey, A.C. Hannon, *Front. Mater.* 4 (2017) 32.
- [5] S. Hosokawa, I. Oh, M. Sakurai, W.-C. Pilgrim, N. Boudet, J.-F. Bézar, S. Kohara, *Phys. Rev. B* 84 (2011) 014201.
- [6] J.T. Gopinath, M. Soljaeiae, E.P. Ippen, V.N. Fuflyigin, W.A. King, M. Shurgalin, *J. Appl. Phys.* 96 (2004) 6931.
- [7] B. Kalken, R.P. Dias, C.-S. Yoo, S.M. Clark, S. Sen, *J. Phys. Chem. C* 118 (2014) 5110–5121.
- [8] J. Troles, V. Shiryayev, M. Churbanov, P. Houzot, L. Brilland, F. Desevedavy, F. Charpentier, T. Pain, G. Sнопatin, J.L. Adam, *Opt. Mater.* 32 (2009) 212–215.
- [9] S.G. Sarwat, Z. Cheng, N. Youngblood, M.S. Alias, S. Sinha, J. Warner, H. Bhaskaran, *Nano Lett.* 19 (10) (2019) 7377–7384.
- [10] I. Valov, R. Waser, J.R. Jameson, M.N. Kozicki, *Nanotechnology* 22 (2011) 254003.
- [11] M.N. Kozicki, H.J. Barnaby, *Semicond. Sci. Technol.* 31 (2016) 113001.
- [12] M.N. Kozicki, M. Park, M. Mitkova, *IEEE Trans. Nanotechnol.* 4 (2005) 331–338.
- [13] J.C. Phillips, *J. Non-Cryst. Solids* 34 (2) (1979) 153–181.
- [14] J.C. Phillips, *J. Non-Cryst. Solids* 43 (2) (1981) 37–77.
- [15] M.F. Thorpe, *J. Non-Cryst. Solids* 57 (3) (1983) 355–370.
- [16] P. Boolchand, *Phys. Rev. Lett.* 57 (1986) 3233.
- [17] W. Bresser, P. Boolchand, P. Suranyi, *Phys. Rev. Lett.* 56 (1986) 2493–2496.
- [18] F. Inam, M.T.M. Shatnawi, D. Tafen, S.J.L. Billinge, P. Chen, D.A. Drabold, *J. Phys.: Condens. Matter* 19 (45) (2007) 455206.
- [19] D.A. Drabold, *Eur. Phys. J. B* 68 (2009) 1–21.
- [20] M. Micoulaut, A. Kachmar, M. Bauchy, S. Le Roux, C. Massobrio, M. Boero, *Phys. Rev. B* 88 (2013) 054203.
- [21] D.N. Tafen, D.A. Drabold, *Phys. Rev. B* 71 (2005) 054206.
- [22] K. Sykina, E. Furet, B. Bureau, S.L. Roux, C. Massobrio, *Chem. Phys. Lett.* 547 (2012) 30–34.
- [23] A. Bouzid, S.L. Roux, G. Ori, M. Boero, C. Massobrio, *J. Chem. Phys.* 143 (3) (2015) 034504.
- [24] C. Massobrio, A. Pasquarello, R. Car, *J. Am. Chem. Soc.* 121 (1999) 2943–2944.
- [25] C. Massobrio, A. Pasquarello, R. Car, *Comput. Mater. Sci.* 17 (2000) 115–121.
- [26] R.F. Rowlands, A. Zeidler, H.E. Fischer, P.S. Salmon, *Front. Mater.* 6 (2019) 133.
- [27] Z. Chaker, G. Ori, C. Tugène, S.L. Roux, M. Boero, C. Massobrio, E. Martin, A. Bouzid, *J. Non-Cryst. Solids* 499 (2018) 167–172.
- [28] A. Becke, *Phys. Rev. A* 38 (6) (1988) 3098.
- [29] C. Lee, W. Yang, R.G. Parr, *Phys. Rev. B* 37 (2) (1988) 785.
- [30] S.R. Elliott, *Physics of Amorphous Materials*, Longman Scientific and Technical, Burnt Mill, Harlow, Essex, England, 1990.
- [31] S. Hosokawa, Y. Kawakita, L. Pusztai, K. Ikeda, T. Otomo, *J. Phys. Soc. Japan* 90 (2021) 024601.
- [32] A. Moharram, A. Abdel-Baset, *Physica B* 405 (2010) 4240–4244.
- [33] M.T.M. Shatnawi, *New J. Glass Ceram.* 05 (2015) 31–43.
- [34] K.D. Machado, J.C. de Lima, C.E.M. Campos, A.A.M. Gasperini, S.M. de Souza, C.E. Maurmann, T.A. Grandi, P.S. Pizani, *Solid State Commun.* 133 (6) (2005) 411–416.
- [35] H. Iyetomi, P. Vashishta, R.K. Kalia, *Solid State Ion.* 32–33 (1989) 954–958.
- [36] P. Vashishta, R.K. Kalia, G.A. Antonio, I. Ebbsjö, *Phys. Rev. Lett.* 62 (1989) 1651–1654.
- [37] H. Iyetomi, P. Vashishta, *Phys. Rev. B* 47 (1993) 3063–3069.
- [38] C. Massobrio, M. Celino, P.S. Salmon, R.A. Martin, M. Micoulaut, A. Pasquarello, *Phys. Rev. B* 79 (2009) 174201.
- [39] M.G. Tucker, D.A. Keen, M.T. Dove, A.L. Goodwin, Q. Hui, *J. Phys.: Condens. Matter* 19 (33) (2007) 335218.
- [40] A. Pandey, P. Biswas, D.A. Drabold, *Sci. Rep.* 6 (2016) 33731.
- [41] A. Pandey, P. Biswas, B. Bhattarai, D.A. Drabold, *Phys. Rev. B* 94 (2016) 235208.
- [42] B. Bhattarai, A. Pandey, D.A. Drabold, *Carbon* 131 (2018) 168–174.
- [43] M.T.M. Shatnawi, C.L. Farrow, P. Chen, P. Boolchand, A. Sartbaeva, M.F. Thorpe, S.J.L. Billinge, *Phys. Rev. B* 77 (2008) 094134.
- [44] P. Lucas, G.J. Coleman, S. Sen, S. Cui, Y. Guimond, L. Calvez, C. Boussard-Pledel, B. Bureau, J. Troles, *J. Chem. Phys.* 150 (1) (2019) 014505.
- [45] Q. Zhou, T. Du, L. Guo, M.M. Smedskjaer, M. Bauchy, *J. Non-Cryst. Solids* 536 (2020) 120006.
- [46] B. Bhattarai, R. Thapa, D.A. Drabold, *Modelling Simulation Mater. Sci. Eng.* 27 (7) (2019) 075002.
- [47] B. Cai, X. Zhang, D.A. Drabold, *Phys. Rev. B* 83 (2011) 092202.
- [48] P.E. Blöchl, *Phys. Rev. B* 50 (1994) 17953–17979.
- [49] G. Kresse, J. Furthmüller, *Phys. Rev. B* 54 (1996) 11169–11186.
- [50] M. Hacene, A. Anciaux-Sedrakian, X. Rozanska, D. Klahr, T. Guignon, P. Fleurat-Lessard, *J. Comput. Chem.* 33 (32) (2012) 2581–2589.
- [51] M. Hutchinson, M. Widom, *Comput. Phys. Comm.* 183 (7) (2012) 1422–1426.

- [52] J.P. Perdew, K. Burke, M. Ernzerhof, *Phys. Rev. Lett.* 77 (1996) 3865–3868.
- [53] P.S. Salmon, *Proc. R. Soc. A* 445 (1924) (1994) 351–365.
- [54] S. Le Roux, A. Bouzid, K.Y. Kim, S. Han, Z. A., P.S. Salmon, C. Massobrio, *J. Chem. Phys.* 145 (8) (2016) 084502.
- [55] E. Gjersing, S. Sen, B. Aitken, *J. Phys. Chem. C* 114 (2010) 8601–8608.
- [56] I. Petri, P.S. Salmon, *Phys. Chem. Glasses* 43C (2002).
- [57] S. King, *Nature* 213 (1967) 1112–1113.
- [58] D.S. Franzblau, *Phys. Rev. B* 44 (1991) 4925–4930.
- [59] S. Le Roux, V. Petkov, *J. Appl. Crystallogr.* 43 (1) (2010) 181–185.
- [60] E. Bergignat, G. Hollinger, H. Chermette, P. Pertosa, D. Lohez, M. Lannoo, M. Bensoussan, *Phys. Rev. B* 37 (1988) 4506–4513.
- [61] W.A. Kamitakahara, R.L. Cappelletti, P. Boolchand, B. Halfpap, F. Gompf, D.A. Neumann, H. Mutka, *Phys. Rev. B* 44 (1991) 94–100.
- [62] P.N. Sen, M.F. Thorpe, *Phys. Rev. B* 15 (1977) 4030–4038.